

Mosaic: Towards Efficient Training of Multimodal Models with Spatial Resource Multiplexing

Yanbo Wang
wang-yanbo@sjtu.edu.cn
Shanghai Jiao Tong University
China
Institute of Artificial Intelligence
(TeleAI), China Telecom
China

Chunyu Xue
dicardo@sjtu.edu.cn
Shanghai Jiao Tong University
China

Quan Chen
chen-quan@cs.sjtu.edu.cn
Shanghai Jiao Tong University
China

Yuxuan Wang
fAKe@sjtu.edu.cn
Shanghai Jiao Tong University
China

Yu Feng
y-feng@sjtu.edu.cn
Shanghai Jiao Tong University
China

Yin Chen
cheny304@chinatelecom.cn
Institute of Artificial Intelligence
(TeleAI), China Telecom
China

Chen Chen*
chen-chen@sjtu.edu.cn
Shanghai Jiao Tong University
China

Anbang Wu
anbang@cs.sjtu.edu.cn
Shanghai Jiao Tong University
China

Qizhen Weng
wengqzh@chinatelecom.cn
Institute of Artificial Intelligence
(TeleAI), China Telecom
China

Abstract

With the wide adoption of Multimodal Models (MMs) in real-world scenarios, it is significant to efficiently train the emerging MMs exhibiting increasingly complex module architectures. For MM deployment, existing works allocate a GPU to only one MM module following a temporal-multiplexing manner; this compromises the training efficiency because a single module often fails to attain high GPU utilization. To improve GPU utilization and attain efficient MM training, we propose to deploy MMs in a temporal-spatial multiplexing manner, allowing multiple MM modules to colocate on a GPU with well-controlled resource quotas. In this paper, we propose *Mosaic*, an efficient MM training system applying temporal-spatial multiplexing. We first develop a flexible and lightweight execution engine that supports MM training with arbitrary resource quotas, and then build a comprehensive and accurate performance model to estimate module execution time under any possible allocation plan. With the performance model, we further adopt powerful heuristics to work out high-quality MM deployment plans in an efficient manner. Testbed experiments confirm that *Mosaic* can effectively improve the training efficiency of popular MMs, with a training speedup of up to 1.31 \times .

1 Introduction

With the rapid development of AI techniques, *Multimodal Models* (MMs) [7, 32, 50, 63] are now widely adopted in many real-world scenarios, especially in edge devices for *autonomous driving* [20, 62, 70] and *embodied intelligence* [10,

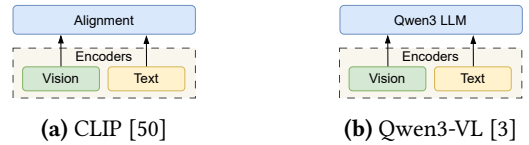


Figure 1. MMs comprise diverse dependent modules.

26, 83]. As shown in Fig. 1, an MM is typically composed of multiple *modules*: input encoders, a shared backbone, and output decoders, forming a directed acyclic graph. In particular, given the deepening adoption of MMs in massive edge scenarios, an emerging trend for MM development is to maintain a modest model size (typical edge-grade MMs are smaller than 10B [6, 26, 28, 73]) yet increase the number of involved modalities (i.e., from two or three modals to *omni-modals* [2, 34, 59]). Moreover, for competitiveness, such MMs often need to be routinely re-trained on the daily-collected data [4, 13, 64, 80], rendering it of paramount significance to train them efficiently with the provisioned GPUs [21, 67].

Given an MM with highly heterogeneous modules, it is challenging to deploy the MM modules over the GPU set for high efficiency. For example, the classical *Megatron-LM* scheme [54] parallelizes each module over all the GPUs, which is inefficient due to the scaling overhead. *DistMM* [21] and *Spindle* [67] schemes instead partition the modules into execution *waves* that temporally multiplex the cluster and, for each wave, minimize the cross-module execution time gap with module-adaptive GPU allocation. However, in those schemes each GPU is *exclusively* allocated to *only one module*

*Corresponding author.

at a time; in modern MMs with heterogeneous modules, some modules with low compute intensity often fail to achieve high utilization with their allocated GPUs, which further leads to compromised training efficiency (Fig. 4).

Therefore, to attain efficient MM training, we need to allow multiple modules to *spatially multiplex* a GPU for improved utilization. That is, overall we need to enforce *temporal-spatial* multiplexing for MM deployment: first map the modules of an MM to sequentially-executed *stages* for temporal GPU multiplexing, and then, within each stage, map each module to a set of compute SMs potentially on multiple GPUs. Ideally, with a proper *MM-stage* and *stage-GPU* mapping plan, we can minimize the cross-module bubbles while attaining high GPU utilization, thereby optimizing the MM training efficiency. In realizing this insight, there are *three key requirements*. First, we need to maintain a flexible execution engine supporting module training with arbitrary SM allocations. Second, we need to build a comprehensive performance model to help evaluate any possible stage-GPU mapping solution. Third, we need to find a high-quality mapping solution in an efficient manner.

In this paper, we propose *Mosaic*, an MM training system that exploits temporal-spatial GPU multiplexing for high efficiency. *Mosaic* is composed of three parts: (1) *Mosaic Multiplexing Engine*—which allows multiple MM modules to arbitrarily multiplex a GPU in a flexible and lightweight manner, (2) *Mosaic Performance Model*—which can accurately estimate the execution efficiency of a module under any possible spatial multiplexing plan, and (3) *Mosaic Mapping Solver*—which can promptly find a high-quality temporal (MM-stage) and spatial (stage-GPU) multiplexing solution.

Specifically, we make non-trivial innovations in each solution aspect. In the *Mosaic Multiplexing Engine*, considering the SM partitioning granularity and isolation overheads, we choose to adopt the *GreenContext* (GC) multiplexing technique [42], which allocates fine-grained SM resources to a module with a separate GC-stream; we also propose *stream-pool pre-creation* to mitigate GC preparation overheads in the critical path. Meanwhile, in the *Mosaic Performance Model*, to support fractional SM allocation on multiple GPUs, we build a comprehensive *scaling surface* for each module; besides, to handle the performance interferences of colocated modules, we add both the *additive* and *multiplicative* rectification items to rectify the performance model, which proves to be more accurate than existing modeling methods. Finally, in the *Mosaic Mapping Solver*, we jointly solve the *MM-stage* and *stage-GPU* mapping problem with high quality by combining the *Greedy Agglomerative Hierarchical Clustering* (GAHC) heuristic with the Google CP-SAT solver; we also incorporate the *early-pruning* and *result-caching* techniques for even better solving efficiency.

We have implemented *Mosaic* with 8K LoCs, and evaluated its performance in a testbed with 32 H100 GPUs. Our end-to-end experiments with popular MMs show that, by

making higher GPU utilization with spatial multiplexing, *Mosaic* improves the training efficiency by up to 1.31× over the state-of-the-art methods. Meanwhile, our deep-dive experiments further confirm that each *Mosaic* innovation—in the multiplexing engine, performance model, as well as mapping solver—does make non-negligible contribution to the overall performance superiority.

In summary, this paper makes three key contributions.

- We identify *temporal-spatial GPU multiplexing* as an effective deployment paradigm for training heterogeneous MMs, where dependent modules temporally share GPUs and parallel modules spatially share SM resources.
- We design *Mosaic*, a practical MM training system that realizes this paradigm through a GreenContext-based multiplexing engine, an interference-aware performance model, and a joint MM-stage/stage-GPU mapping solver.
- We implement *Mosaic* and demonstrate on a 32-H100 testbed that it improves training efficiency by up to 1.31× over state-of-the-art MM training schemes.

2 Background and Motivation

2.1 Multimodal Models: The Emerging Trend

Multimodal Models (MMs), which jointly process inputs of diverse forms (e.g., *text*, *vision*, and *audio*) [1, 15, 32], are increasingly significant for diverse scenarios like *embodied intelligence* [31] and *autonomous driving* [76]. As illustrated in Fig. 1 and Fig. 2, an MM is composed of multiple (encoder, decoder, and backbone) modules with mutual dependencies, which form a *Directed Acyclic Graph* (DAG). For example, *CLIP* [50] is a classical MM that aligns the features of different modalities via contrastive learning, and *Qwen3-VL* [3] uses an LLM backbone to merge the inputs respectively from the *vision* and *text* encoders.

In particular, given the widespread and also in-depth adoption of MMs in many real-world application scenarios [37, 57, 61]—where the MMs are increasingly deployed on *edge hardware* like cars, robots, and phones [26, 53, 56, 74, 81], the recent days have witnessed a *trend* to develop *modest-size yet high-modal-complexity* MMs: maintaining a modest size allows the MM to be hosted by low-end edge devices, and supporting more modalities can make the MM more powerful for realistic tasks. Fig. 2 shows such MM examples. *Image-Bind* [16] aligns 6 modalities (*image*, *text*, *audio*, *depth*, *thermal* and *IMU*) into one embedding space, *Unified-IO 2* [35] combines 5 encoders and 3 decoders with an LLM backbone, and *OFASys* [2] integrates 9 encoders and 6 decoders with a universal model. As revealed by Table 1, those modules have strong architecture heterogeneity. Moreover, as shown in Fig. 2d, in some cases multiple MMs may work together on a shared device [31, 69], which also form a *logically-complex* MM requiring joint training.

Meanwhile, for competitiveness, MMs need to be timely refreshed with routinely collected data. Recent studies already

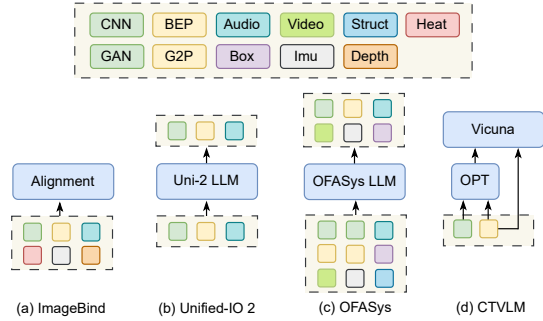


Figure 2. Edge-grade MMs with high modal complexity.

Model	Module	Layers	Dim.	TFLOPs	CI
Qwen3-VL (8.1B)	Qwen3LLM	36	4096	22.27	145.2
	Vision	27	4096	2.58	82.4
	Text	1	4096	0.15	2.1
Unified-IO 2 (3.8B)	UIO-2 LLM	48	3072	16.70	110.5
	Vision	11	768	1.48	24.6
	Audio	11	768	1.06	21.8
ImageBind (1.2B)	Vision	24	1024	4.17	35.2
	Audio	12	768	2.09	22.8
	Text	12	768	1.04	20.5
OFASys (6.3B)	OFASys LLM	36	1280	4.80	41.6
	Vision	8	1280	1.35	18.2
	Text	4	1280	0.72	12.5
	Audio	6	1280	0.95	14.8

Table 1. Architecture information of representative MMs (for TFLOPs information, the input configuration is the same as in Table 2). *Compute intensity* (CI) is measured in FLOPs/Byte.

report treating MM updating as daily workloads: FoMo-in-Flux [64] and D-MoLEs [14] have both focused on *continual MM training* in real-world scenarios, and Modyn [4] has further explored how to orchestrate *recurring* model updates in data-centric pipelines. Hence, it is *increasingly significant* to train MMs *efficiently* with the provisioned GPU set.

2.2 Efficiency-oriented MM Deployment

Optimizing model deployment for high training efficiency is a classical research problem in the literature, yet it remains challenging for MMs comprising heterogeneous modules organized in DAGs. Essentially, deploying a DAG-structured MM involves two decision aspects: (1) how to deploy the *dependent* modules, and (2) how to deploy the *parallel* modules. Here, we walk through existing deployment methods concerning the two aspects.

Deploying dependent MM modules. Regarding the deployment of dependent MM modules, the data dependencies between upstream and downstream modules prevent their concurrent execution. For conventional *Large Language*

Models (LLMs) typically of a large size, the dependent modules (aka model layers) are often deployed in GPU clusters following the *Pipeline Parallel* (PP) paradigm [22, 39]. However, PP deployment incurs *warm-up* and *cool-down* bubbles which waste the GPU resources; for our targeting *edge-grade MMs* which are not large (and can thus be kept in GPU memory during training), it would be more efficient to have them *temporally-multiplex* the GPUs [21, 54, 67], such that no GPUs have to stand by idly waiting for the output of upstream modules. Then we turn to deploying the *parallel* modules, which are particularly challenging for MMs due to the substantial module heterogeneity.

Deploying parallel MM modules. Regarding the deployment of parallel (yet heterogeneous) MM modules, a series of works have been proposed in the literature. As illustrated in Fig. 3a, the classical *Megatron-LM* framework [54] adopts a symmetric allocation strategy, copying each module to all the provisioned GPUs following the *Data Parallel* (DP) paradigm [30] (different modules are still executed sequentially via temporal multiplexing). Although straightforward, this paradigm is often inefficient: the usually over-aggressive parallelization would amplify the communication-to-computation ratio and incur remarkable per-module execution slowdown.

To address such inefficiency, later MM deployment works enable *asymmetric, module-adaptive* GPU allocation. As shown in Fig. 3b, *DistMM* [21] assigns disjoint sets of GPUs to different modules (each module still enforces DP over its allocated GPUs). Its objective is to balance the execution times of parallel modules; however, because resource allocation is restricted to integer GPU counts, the training system frequently suffers from sub-optimality due to rounding error. These errors may leave substantial duration misalignment between modules, resulting in resource idle time prior to the cross-module data-merging barriers. To further alleviate such rounding-caused module duration inconsistency, as shown in Fig. 3c, *Spindle* [67] proposes to decompose the modules into finer-grained slices. Note that, although this improved granularity allows for better temporal alignment, it comes at the cost of significantly higher programming complexity and increased coordination overhead due to the frequent synchronization required between slices.

Common limitations of existing deployment paradigms. However, despite the differences, the aforementioned paradigms commonly exhibit a fundamental limitation: they assign each GPU to only one MM module, assuming that *each module must exclusively occupy the GPUs allocated to it*; such an allocation restriction inherently compromises the resultant MM training efficiency.

In fact, it often occurs that a single MM module fails to attain high utilization on the GPUs allocated to it. Specifically, in Table 1, we list the module-level architecture information

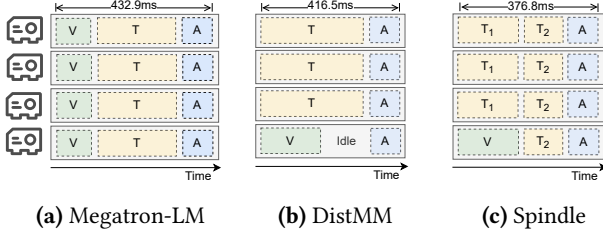


Figure 3. Behaviors of different MM deployment schemes when training the CLIP model on four GPUs. V , T , and A denote *vision-encoder*, *text-encoder* and *alignment* modules.

of typical MMs, including their *Compute Intensity* (CI). Table 1 suggests that the per-module compute intensity can vary by over *an order of magnitude* across different modules, exhibiting strong cross-module heterogeneity. For example, for the Qwen3-VL-8B model, the *text-encoder* module has a CI of 2.1 FLOPs/Byte, the *vision-encoder* module has a CI of 82.4 FLOPs/Byte, yet the LLM backbone as a module has a CI of 145.2 FLOPs/Byte. In the meantime, modern GPUs feature hundreds of *streaming multiprocessors* (SMs) [41], and a module with low CI usually fails to fully monopolize those SMs, thereby yielding low GPU utilization.

By contrast, by relaxing the exclusive GPU allocation constraint, we can potentially attain higher GPU utilization and further yield faster MM training. As shown in Fig. 4a, with modern spatial multiplexing techniques [40, 42, 43], we can colocate multiple MM modules on a GPU. By properly allocating a portion of the GPU SMs to each module based on its computing characteristics, it is possible that each colocated module can complete at around the same time. In this way, the provisioned GPUs can (1) avoid temporal resource wastage while (2) attaining higher utilization during their busy time. To confirm, we train the CLIP model on a 4×H100 GPU server under different deployment paradigms. As revealed by Fig. 4b, compared to those existing paradigms in Fig. 3, a *spatial-multiplexing-enabled* deployment solution illustrated in Fig. 4a can indeed attain a higher GPU utilization (with an improvement of 29.9% over the status quo *Spindle* paradigm) and further a shorter iteration time. This result confirms the necessity to enable spatial GPU multiplexing in MM deployment.

Insight. In summary, when training MMs comprising heterogeneous modules, we need to exploit *temporal-spatial GPU multiplexing* for best training efficiency. For *dependent* MM modules, we need to adopt *temporal* GPU multiplexing to avoid resource bubbles; more importantly, for *parallel* MM modules, we need to adopt *spatial* GPU multiplexing to enhance the GPU utilization. Next, we will explore how to enforce this insight into practice.

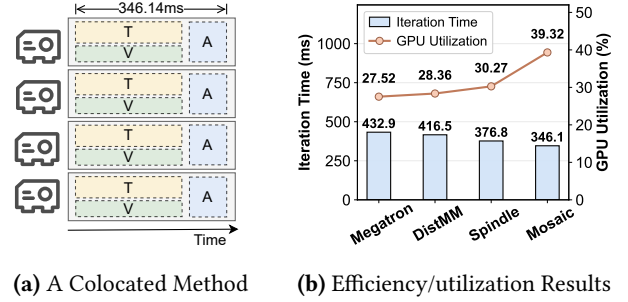


Figure 4. Benefits of spatial GPU multiplexing. Allowing vision (V) and text (T) encoders to colocate reduces total iteration time and improves overall GPU utilization.

3 Mosaic Solution Design

In this section, we present the design details of *Mosaic*, an MM training system exploiting *temporal-spatial GPU multiplexing* for high compute efficiency. We will first mathematically formulate the problem and make the system overview in Sec. 3.1, and then we elaborate each design component in Sec. 3.2, Sec. 3.3, and Sec. 3.4. Finally, we discuss some peripheral design issues in Sec. 3.5.

3.1 Problem Formulation and System Overview

Problem formulation. For clarity, we first formulate the problem of efficiency-oriented MM deployment. We represent each MM training job as a DAG, $\langle \mathcal{M}, \mathcal{E} \rangle$, where \mathcal{M} denotes the MM *modules* and \mathcal{E} denotes the data *dependencies* between modules. Under the temporal-spatial multiplexing mode, MM training needs to be executed in sequential *stages*, each comprising a set of parallel modules: modules in different stages temporally multiplex the GPU resources, whereas modules within a stage spatially multiplex the GPU resources. Following this mode, the MM deployment problem can be expressed as conducting *two-level* mappings: (1) *MM-stage mapping*—map the MM modules to temporally ordered stages with the module dependency preserved, and (2) *stage-GPU mapping*—map the parallel modules of each stage to the GPU resources with fine-grained SM allocation enabled. Next, we respectively formulate the two mapping problems.

1) *Formulating the outer MM-stage mapping problem.* Suppose the execution plan consists of n (n is also a decision variable) stages $\mathcal{S} = \langle S_1, S_2, \dots, S_n \rangle$, which are executed sequentially on a pool of GPU resources \mathcal{G} . We let $T_{\text{iteration}}$ represent the training iteration time which is the optimization target, then the MM-stage optimization problem can be formulated as:

$$T_{\text{iteration}}^*(\mathcal{M}, \mathcal{G}) = \min_{n, \mathcal{S}=(S_1, S_2, \dots, S_n)} \sum_{i=1}^n T_{\text{stage}}^*(S_i, \mathcal{G}), \quad (1)$$

$$\text{s.t.} \quad \bigcup_{i \in [n]} S_i = \mathcal{M}, \quad (2)$$

$$\mathcal{S}^{-1}(m) < \mathcal{S}^{-1}(m'), \quad \forall (m, m') \in \mathcal{E}. \quad (3)$$

The objective formula (1) means to minimize total iteration time, which, given the temporal multiplexing nature, is modeled as the sum of all stages' execution times. Here $T_{\text{stage}}^*(S_i, \mathcal{G})$ means the shortest possible execution time of stage S_i given the GPU set \mathcal{G} , which is obtained by solving the later stage-GPU mapping problem. The constraint formula (2) states that all modules are covered, and formula set (3) ensures the data dependency is complied with by the mapping plan, where $\mathcal{S}^{-1}(m)$ denotes the index of the stage that contains module m .

2) *Formulating the inner stage-GPU mapping problem.* In solving the above optimization problem, for each candidate MM-stage mapping solution (i.e., fixing S_i and \mathcal{G}), we need to acquire $T_{\text{stage}}^*(S_i, \mathcal{G})$ —the shortest stage execution time attained under the optimal module deployment (stage-GPU mapping) plan. Specifically, we let $a_m^g \in [0, 1]$ be the SM quota of GPU g allocated to module m , $\mathcal{A} = \{a_m^g\}_{m \in \mathcal{S}}^{g \in \mathcal{G}}$ be the overall stage-GPU mapping plan, and $T_{\text{module}}(m, \mathcal{A})$ be the execution time of module m . Then the stage-GPU mapping problem can be formulated as:

$$T_{\text{stage}}^*(S, \mathcal{G}) = \min_{\mathcal{A}=\{a_m^g\}_{m \in \mathcal{S}}^{g \in \mathcal{G}}} \max_{m \in \mathcal{S}} T_{\text{module}}(m, \mathcal{A}) \quad (4)$$

$$\text{s.t.} \quad \sum_{m \in \mathcal{S}} a_m^g \leq 1, \quad \forall g \in \mathcal{G}. \quad (5)$$

The objective formula (4) aims to minimize the end-to-end stage latency, estimated as the slowest module's latency. Constraint formulas (5) prevent over-allocation of computation resources. The memory resource constraint can be formulated similarly; it is omitted here for simplicity, but always complied with in practice. Note that existing methods like *DistMM* and *Spindle* essentially restrict the allocation a_m^g to binary values $\{0, 1\}$, and from a mathematical point of view, such a solution space restriction naturally compromises the solution quality.

Challenges. While the above formulas clearly depict what an ideal solution should be, it is still difficult to find and apply that optimal solution in practice. Specifically, there are three challenges.

- First, to support spatial multiplexing with controlled GPU quota, we need to prepare a flexible and light-weight training engine that can execute MM modules with arbitrary SM allocation amounts. While modern GPUs support a series of spatial multiplexing

techniques [40, 42, 43], they, however, lack the allocation amount flexibility or bring large overheads when preparing the desired SM execution slots for MM modules in each stage.

- Second, to solve the above optimization problems, a prerequisite is to obtain a comprehensive performance model, $T_{\text{module}}(m, \mathcal{A})$, that can estimate the execution time of a module when colocated with other modules at arbitrary resource ratios. However, with partial GPU allocation allowed, the performance modeling space is much larger than existing ones; worse, due to complicated interferences among colocated modules, it is hard to accurately predict the module performance for arbitrary colocating plans.
- Third, it also presents a non-trivial challenge to solve the formulated problems in a practical manner. Given the increasing MM complexity and the nested nature of the two optimization problems, the solution space is highly complex, and it is hard to find a high-quality deployment solution within a modest time budget.

To harvest the benefit of temporal-spatial multiplexing in real-world MM deployments, we need to address all three challenges in our proposed system.

System overview. As shown in Fig. 5, we develop *Mosaic*, an MM training system that exploits temporal-spatial GPU multiplexing for high training efficiency. *Mosaic* is composed of three components: the *Mosaic Multiplexing Engine*, the *Mosaic Performance Model*, and the *Mosaic Mapping Solver*.

- First, the *Mosaic Multiplexing Engine* supports module training with an arbitrary number of SMs on a GPU. To support such flexibility while being light-weight for runtime use, we adopt the *Green Context* (GC) technique and further propose *GC-stream pool pre-creation* to amortize the maintenance overheads.
- Second, the *Mosaic Performance Model* can accurately estimate the execution time of an MM module when it is allocated any number of GPU SMs and colocated with any MM modules. We build a *scaling surface* for comprehensive modeling and also incorporate the *additive* and *multiplicative* interference items for accurate modeling.
- Third, the *Mosaic Mapping Solver* can efficiently find a high-quality temporal (MM-stage) and spatial (stage-GPU) multiplexing plan for an MM. It combines the *Greedy Agglomerative Hierarchical Clustering* (GAHC) heuristic with the *CP-SAT* solver to get high-quality solutions, and also adopts *early-pruning* and *result-caching* techniques to further enhance the solving efficiency.

Next, we elaborate on the solution design in each *Mosaic* component in greater detail.

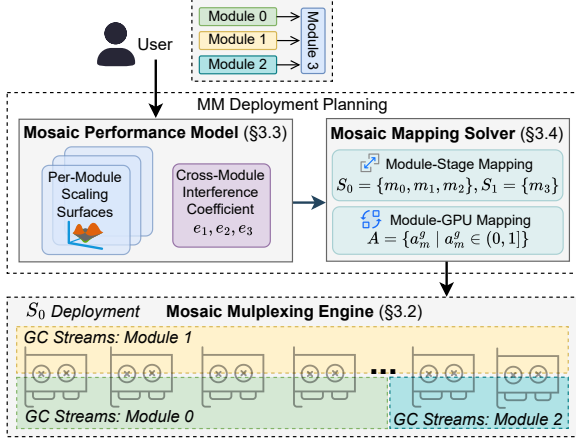


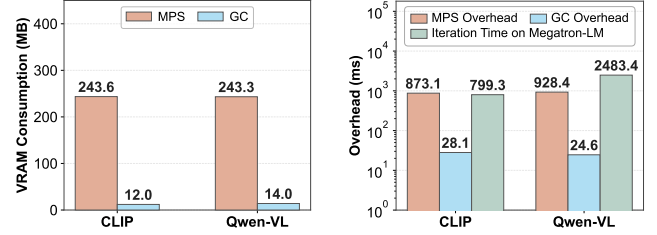
Figure 5. Overview of our Mosaic system.

3.2 Flexible and Light-weight Spatial Multiplexing

To exploit spatial multiplexing for efficient MM training, we need to first provide a flexible training runtime. Specifically, that runtime should (1) support *arbitrary partitioning* of a GPU’s computing resources to different MM modules—per the solution requirement of Eq. 4. Moreover, as indicated in Fig. 4a, that GPU partitioning scheme should (2) be *dynamically-tunable* during the training process—given the periodical occurrence of stage transitions.

Choosing among popular multiplexing techniques for best flexibility. Based on the two requirements above, we surveyed the popular spatial multiplexing techniques supported by modern NVIDIA GPUs. The Multi-Instance GPU (MIG) [40] technique can partition a GPU into up to seven instances, each fully isolated with its own memory, cache, and compute cores. However, the MIG technique cannot partition GPU SMs at arbitrary portions (must follow fixed configurations). Meanwhile, Multi-Process Service (MPS) [43] is a classical spatial multiplexing technique that allows allocating an arbitrary number of GPUs to a *process* (i.e., a MM training job in our problem). However, MPS itself does not support fine-grained, intra-process resource isolation at per-module level. Recently, *Green Context* (GC) [42] has been developed as an advanced spatial multiplexing technique that supports intra-process SM isolation at CUDA stream level; besides, as shown in Fig. 6, its memory and time overheads are much less than MPS. Therefore, we choose to adopt the GC techniques in *Mosaic*: by mapping a MM module to a CUDA-stream with designated SM quota, we can realize module-level adaptive GPU resource allocation.

Light-weight allocation adjustment with a pre-created stream pool. While Green Context supports fine-grained GPU multiplexing, once a GC stream is launched, its SM quota can however not be adjusted at runtime. Therefore, we need to prepare a distinct Green Context stream (GC-stream)



(a) VRAM overhead comparison between MPS and Green Context. Green Context achieves the least overhead, with a latency of fewer memory overhead. (b) Latency overhead comparison. Green Context features 95% less overhead, with a latency of less than 30 ms.

Figure 6. Green Context is lightweight in both memory and time overhead.

for each module with the desired SM quota. Nonetheless, creating or destroying such GC-stream would incur non-negligible overheads in the critical path (e.g., for reclaiming the stream objects as well as the associated GC states). Our later testbed evaluations (Fig. 11b) show that, when training the Imagebind model on $8 \times \text{H100}$, it takes up to 6.63% of the per-iteration time to manage the GC-streams in a on-demand (create-and-then-destroy) manner. Such overheads would be substantial when conducting stage transition for multiple times within each MM training iteration.

Therefore, to eliminate stream preparation overheads in the critical path, we choose to create a Green Context *stream pool* in advance. Moreover, we note that MM training is an iterative process where the same spatial-colocation plan would be repeated in each iteration. That is, given the MM modules and the available GPUs, all the desirable GC-stream configurations to appear is essentially a white-box information—acquirable with offline profiling. Therefore, in our *Mosaic* system, we pre-create—at training commencement—a pool of GC-streams-to-use with the desired SM quotas; once a training stage completes in an iteration, the modules of the next training stage can be immediately launched, without incurring any stream-creation/destruction delay in the critical path. This way, we can make flexible and light-weight resource provisioning at per-module granularity, well supporting the enforcement of our solution paradigm.

3.3 Thorough and Accurate Performance Modeling

With spatial sharing enabled, a MM module can be allocated an arbitrary SM portion on each GPU: $a_m^g \in [0, 1]$. This, however, complicates the estimation of $T_{\text{module}}(m, \mathcal{A})$ (the latency of module m under allocation \mathcal{A}) for two reasons: (1) The allocation space expands from a discrete set of GPU counts to a continuous multi-dimensional surface, making exhaustive profiling infeasible; (2) Spatial sharing introduces complex interference patterns when modules are

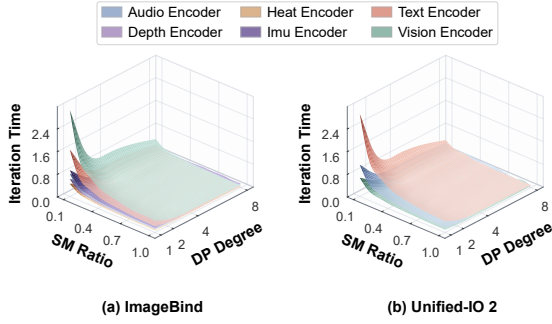


Figure 7. MM modules’ scaling curves are smooth with respect to DP Degree and SM Ratio.

collocated onto the same GPU. These challenges render existing solutions inadequate and here we respectively address them.

Towards comprehensive modeling with symmetry-based solution pruning and smoothness-based grid sampling.

To overcome the first challenge, *Mosaic* builds a *scaling surface* through symmetry-based pruning and smoothness-based sampling. While *Mosaic* theoretically allows a module to receive heterogeneous SM quotas across different GPUs, such asymmetric configurations are inherently suboptimal for data-parallel replicas: synchronous iterations are limited by the slowest worker, any asymmetry creates stragglers and results in wasted resource cycles on faster GPUs. Consequently, we prune the search space by enforcing symmetric allocations. Let $\mathcal{G}_m = \{g \in \mathcal{G} \mid a_m^g > 0\}$ be the set of GPUs assigned to module m , and $d_m = |\mathcal{G}_m|$ be its data-parallel degree, we then require that:

$$\forall m, \exists a_m, \forall g \in \mathcal{G}_m, \quad a_m^g = a_m. \quad (6)$$

By enforcing a uniform quota a_m across all d_m replicas, we effectively collapse the high-dimensional allocation mesh into a tractable two-dimensional space – each module’s deployment is thus simplified to a tuple (d_m, a_m) .

Since empirical observations in Fig. 7 show that latency varies smoothly along both dimensions, *Mosaic* approximates this surface with sparse grid sampling rather than exhaustive measurement. Specifically, we profile d_m at powers-of-two (e.g., 1, 2, 4, 8) and a_m at *decile* increments (i.e., 0.1, 0.2, ..., 1.0). This sparse mesh provides a high-fidelity approximation of the scaling surface $T_{\text{module}}(m, \mathcal{A}) = \int_m^{\text{scaling surface}}(d_m, a_m)$ while reducing profiling overhead by orders of magnitude, striking a practical balance between model accuracy and characterization efficiency.

Performance model rectification with awareness to I/O interferences. To address the second challenge—the non-linear interference arising from co-location—*Mosaic* incorporates an I/O-aware correction mechanism into its

performance model. The scaling surface $T_{\text{module}}(m, d_m, a_m)$ constructed via grid sampling primarily captures compute-bound (SM) contention. However, MM modules are also significantly I/O-intensive. Under the NVIDIA GC mechanism, co-located modules share a common GPU memory plane, making memory bandwidth contention a major source of execution inefficiency. As illustrated in Fig. 8a, even with a fixed SM quota a_m , a module’s computing efficiency fluctuates remarkably as the available memory bandwidth varies. As in Fig. 8a, when the text-encoder’s compute quota is fixed, increasing the co-located audio-encoder’s compute quota aggravates bandwidth contention and further prolongs the text-encoder’s iteration time.

To model this without exhaustive profiling of module collocation combinations, we use memory bandwidth utilization $B(m, a_m) \in [0, 1]$ as a generic interference proxy. This metric is collected concurrently during grid sampling at no extra cost. We then adjust the baseline latency by an I/O interference term Δ_m^g ; for a module spanning multiple GPUs \mathcal{G}_m , the execution time is governed by the worker encountering the maximum delay:

$$T_{\text{module}}^{\text{rectified}}(m, \mathcal{A}) = T_{\text{module}}(m, \mathcal{A}) + \max_{g \in \mathcal{G}_m} \Delta_m^g. \quad (7)$$

The remaining question is how to estimate the delay Δ_m^g when multiple modules are co-located on the same GPU. We observe that linear approximations of aggregate utilization—used in works like LLMStation [19]—fail to capture high-intensity contention. Specifically, as shown in Fig. 8b, the additive-only model attains only $R^2 = 0.86$ whereas ours reaches 0.97 (R^2 is the *coefficient of determination* [9], and a value closer to 1 indicates a better fitting performance), because it underestimates the rapidly increasing runtime when aggregate bandwidth pressure approaches saturation.

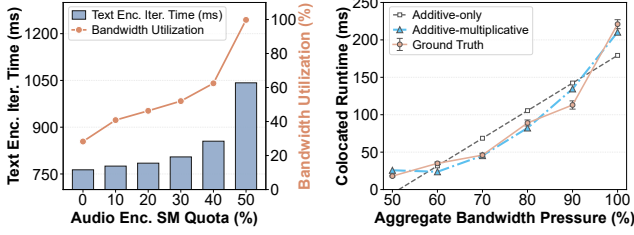
Consistent with recent studies [55, 79], we find that marginal interference is often multiplicatively augmented by the resource demands of peers. We therefore employ a composite formulation to fit the universal interference coefficients e_1, e_2, e_3 :

$$\Delta_m^g = e_1 + e_2 \sum_{m \in \mathcal{M}_g} B(m, a_m) + e_3 \prod_{m \in \mathcal{M}_g} B(m, a_m), \quad (8)$$

where $\mathcal{M}_g = \{m \in S_i \mid g \in \mathcal{G}_m\}$ is set of modules co-located on GPU g . As shown in Fig. 8b, this additive-multiplicative approach accurately tracks non-linear degradation, providing the high-fidelity estimation required for optimal allocation.

3.4 Efficient and High-quality Decision Making

With the ability to accurately estimate $T_{\text{module}}(m, \mathcal{A})$, we can now turn to the scheduling problem as defined in Sec. 3.1. *Mosaic* needs to partition modules into an ordered list of stages $\mathcal{S} = \langle S_1, S_2, \dots, S_n \rangle$, where each stage $S_i \subseteq \mathcal{M}$ contains modules that execute in parallel, and the stage order respects every dependency in \mathcal{E} . For each stage S_i , *Mosaic* must also choose an optimal allocation plan \mathcal{A}_{S_i} over the



(a) Increasing SM quota of the colocated text-encoder and audio-encoder affects efficiency and overall bandwidth utilization. (b) Estimated text-encoder performance with the *additive-only* and *additive-multiplicative* methods, plus the ground truth.

Figure 8. Memory bandwidth contention does degrade performance, and simple linear modeling is insufficient. We train two modules (text-encoder and audio-encoder) from the OFASys model on an H100 GPU.

GPU set \mathcal{G} to minimize stage latency. The resulting iteration time is $T_{\text{iteration}}(\mathcal{S}, \mathcal{G}) = \sum_{S_i \in \mathcal{S}} T_{\text{stage}}(S_i, \mathcal{G})$.

This decision has two coupled levels. The upper level decides which independent modules should be grouped into the same stage, while the lower level decides whether the modules inside a candidate stage can be placed onto the available GPUs with acceptable latency. The coupling makes exhaustive search intractable: the number of possible stage partitions grows as the Bell number of $|\mathcal{M}|$, and each partition still requires solving a complex per-stage resource mapping problem. *Mosaic* address this with Alg. 1 which we will detail next.

A high-quality algorithm to solve Problem 4: combining GAHC heuristic with CP-SAT solver. *Mosaic* starts from a conservative stage list in which every module forms its own stage (Line 1). In each round, it considers all pairs of current stages that can be legally merged without violating the dependency order. For a candidate merge $S_x \cup S_y$, *Mosaic* invokes `STAGEEVAL` to compute the optimal latency $T_{S_x \cup S_y}$ and the corresponding optimal allocation $\mathcal{A}_{S_x \cup S_y}$. The merge benefit is

$$\Delta(S_x, S_y) = T_{S_x} + T_{S_y} - T_{S_x \cup S_y}. \quad (\text{Line 12}) \quad (9)$$

Mosaic applies the merge with the largest positive Δ ; if no merge can further reduce the iteration time, the search terminates (Line 15~18). This greedy merging is an instance of *Greedy Agglomerative Hierarchical Clustering* (GAHC), a classical heuristic for progressive grouping.

For each candidate stage proposed by the upper-level GAHC search, `STAGEEVAL` solves the optimal intra-stage allocation (i.e., Eq. (4)). Its min-max objective is hard to hand to a standard optimization solver as-is, so we apply binary search on a scalar target latency τ and convert it into repeated feasibility tests. For each trial τ , we collect,

Algorithm 1 *Mosaic*'s Temporal-Spatial Mapping Solver

Require: MM DAG $\langle \mathcal{M}, \mathcal{E} \rangle$, GPU set \mathcal{G}

Ensure: Stage list \mathcal{S} and allocations $\langle \mathcal{A}_{S_1}, \dots, \mathcal{A}_{S_n} \rangle$

```

1:  $\mathcal{S} \leftarrow \langle \{m\} \mid m \in \mathcal{M} \rangle$  in a topological order
2: for all  $S \in \mathcal{S}$  do
3:    $(T_S, \mathcal{A}_S) \leftarrow \text{STAGEEVAL}(S, \mathcal{G})$ 
4: while  $|\mathcal{S}| > 1$  do
5:    $\Delta_{\text{best}} \leftarrow 0$ ;  $\text{Best} \leftarrow \perp$ 
6:   for all  $(S_x, S_y) \in \text{Pairs}(\mathcal{S})$  do
7:     if merging  $S_x$  and  $S_y$  violates  $\mathcal{E}$  then
8:       continue
9:     if EARLYPRUNE  $(S_x, S_y, \Delta_{\text{best}})$  then
10:      continue
11:      $(T_{S_x \cup S_y}, \mathcal{A}_{S_x \cup S_y}) \leftarrow \text{STAGEEVAL}(S_x \cup S_y, \mathcal{G})$ 
12:      $\Delta \leftarrow T_{S_x} + T_{S_y} - T_{S_x \cup S_y}$ 
13:     if  $\Delta > \Delta_{\text{best}}$  then
14:        $\Delta_{\text{best}} \leftarrow \Delta$ ;  $\text{Best} \leftarrow (S_x, S_y)$ 
15:   if  $\text{Best} = \perp$  then
16:     break
17:    $(S_x, S_y) \leftarrow \text{Best}$ 
18:   Apply merge of  $S_x$  and  $S_y$  in  $\mathcal{S}$ .
19: return  $\mathcal{S}, \langle \mathcal{A}_S \mid S \in \mathcal{S} \rangle$ 

```

for every module, the deployment options whose predicted latency meets the target τ , then ask whether one option per module can be selected and placed within the resource constraints. This joint selection-and-placement check is devised as a multi-constraint feasibility problem and solved with established CP-SAT [47] engine. The smallest feasible τ is exactly $T_{\text{stage}}(S, \mathcal{G})$.

Additionally, we set a tunable hyperparameter *SM-quota search granularity* to discretize each module's fractional SM quota into candidate allocation levels. Empirically, we set it to 10% and justify this choice in the Sec. 5.4.

Enhancing algorithm efficiency with early-pruning and result-caching. The preceding procedure yields high-quality mappings, but it is far from fast in practice, largely because evaluating candidate merges repeatedly invokes `STAGEEVAL`. We therefore apply *early-pruning* and *result-caching* to cut this cost.

First, *early-pruning* (Line 9 in Alg. 1) drops candidate merges that cannot possibly beat the best merge gain Δ_{best} already found in the current greedy round. Before running `STAGEEVAL`, we test whether each module in the would-be merged stage still has a *non-empty* set of deployment options under which a merge gain strictly larger than Δ_{best} is attainable; if any module fails, the pair cannot outperform Δ_{best} and we skip the relatively costly full CP-SAT solver call.

Second, *result-caching* (Line 11 in Alg. 1) memorizes the outcome of `STAGEEVAL`. We store the solved latency and

allocation (T_S, \mathcal{A}_S) the first time a stage composition S appears and return the cached entry on later requests. This is well motivated: the outer greedy loop runs for many rounds and evaluates a large number of candidate merges per round, while committing to only *one* merge at the end of each round, so the same intermediate stage compositions are revisited often—yielding plentiful cache hits and avoiding repeated CP-SAT work for identical module sets.

With the above two techniques, we can effectively reduce search overhead while preserving the solution quality, which will be confirmed by our evaluations later in Sec. 5.3.3.

3.5 Discussions

Impact of data heterogeneity. Data heterogeneity is a hot research topic for MM training, which manifests in two aspects: *intra-modal* heterogeneity and *inter-modal* heterogeneity. We note that they do not affect the effectiveness of *Mosaic*. Regarding intra-modal (sample-length) heterogeneity, a series of data preparation techniques, like *padding* [27], *truncation* [48] and *pruning* [52], are commonly used in mainstream training practices [7, 68, 78]. We follow such practices and ensure that the ultimate inputs of a module have the same length. Regarding inter-modal (sample-format) heterogeneity, we note that its impact has already been priced in when building our module-specific performance models: the module execution time is jointly affected by the module size, sample format and batch size, all of which are fixed during the training process and thereby well captured by *Mosaic*.

Compatibility with pipeline parallelism. While in this paper we focus on modest-size edge-grade MMs where *pipeline parallelism* (PP) [22, 39] is inappropriate (Sec. 2.2), for cloud-hosted cutting-edge MMs with hundreds of billions of parameters [17, 38, 45, 49, 77], PP deployment would be unavoidable, which means to host the encoders/decoders and LLM backbones in separate GPU sets—each forming a pipeline stage. We note that our temporal-spatial multiplexing principle can still be applied together with PP. With colocated module execution, we can enhance the GPU utilization of the encoder/decoder modules. In that sense, some of their allocated GPUs can be yielded to other pipeline stages, which, with proper load balancing methods [65, 66], can help to further improve the end-to-end pipeline execution time.

Extensibility to inference workloads. When serving MM inference requests, the problem also exists that a single MM module fails to utilize the allocated GPU. Moreover, in some scenarios, a single input sample may trigger multiple MM inference tasks: for example, in V-Bench [23] evaluation, a video sample is processed by multiple MM raters (e.g., DINO [5], ViT [8] and RAFT [60]). In such cases, it is appealing to further enable *cross-MM* module collocation to improve the overall benchmarking efficiency. That said, we note that the research challenges for inference workloads are different. Different from training scenarios, in typical

inference scenarios, the batch size is determined by the runtime request intensity; such batch size uncertainty yields a larger performance modeling space. Meanwhile, the solution paradigm would also be different (e.g., batch size and resource provisioning plan may also be part of the solution).

4 Implementation

Mosaic is implemented with $\sim 8\text{K}$ lines of code, including *Mosaic Multiplexing Engine* with $\sim 3\text{K}$ LoC, *Mosaic Performance Model* with $\sim 3\text{K}$ LoC, and *Mosaic Mapping Solver* with $\sim 2\text{K}$ LoC. *Mosaic Multiplexing Engine* is a PyTorch-based [46] distributed runtime. It manages module-specific communication groups and reuses them across stages to avoid unnecessary communicator initialization. It also implements the CUDA stream pooling optimization as described in Sec. 3.2. *Mosaic Performance Model* conducts profiling for each module, sweeping chosen DP degrees and SM quotas, recording iteration time, GPU memory usage, SM utilization, and memory bandwidth utilization into structured JSON files, and further manages scaling curve fitting. *Mosaic Mapping Solver* implements Alg. 1 with Google OR-Tools CP-SAT [47], encoding group selection, GPU placement, and SM-quota assignment as integer variables with memory under SM-capacity constraints. It stores collocation groups as module bitmasks to realize result-caching for STAGEVAL, and also applies early-pruning for merging candidates before calling the solver.

5 Evaluation

This section evaluates *Mosaic* performance on representative MM training workloads over state-of-the-art baseline methods (Sec. 5.1). The end-to-end performance results in Sec. 5.2 suggest that *Mosaic* can remarkably improve the training efficiency and GPU utilization. Further microscopic studies in Sec. 5.3 demonstrate the effectiveness of each of *Mosaic*'s core design innovations. In Sec. 5.4 we conduct sensitivity studies to evaluate *Mosaic* performance across diverse resource scales and SM-quota search granularity.

5.1 Experimental Setup

Hardware. All experiments are conducted on a GPU cluster consisting of 4 HGX nodes, each equipped with 8 NVIDIA H100 (80GB) GPUs and 64 Intel(R) Xeon(R) Platinum 8468 CPU cores. The CUDA version is 13.0. Within each node, GPUs are connected by NVLink with 900 GBps bandwidth. Across nodes, RDMA communication is provided by 8 InfiniBand NICs per node, each with 400 Gbps bandwidth.

Models. In our experiments, we respectively train six representative MM models: *CLIP* [50], *Qwen3-VL* [3], *Unified-IO 2* [35], *ImageBind* [16], *OFASys* [2], and *CTVLM* [36]. All of them are elaborated in Sec. 2.1. In particular, *Unified-IO 2*, *ImageBind*, and *OFASys* each can be viewed as a model *family*, in which, depending on the multi-modal tasks, the modules

Modality	Parameter	Value
Text	Sequence length	2048 tokens
Image	Resolution	512×512
	Channels	RGB
Video	Frames	32
	Resolution	512×512
Audio	Sampling rate	16 kHz
	Duration	8 s
Depth	Resolution	224×224
Thermal	Resolution	256×256
IMU	Axes	6
	Sampling rate	100 Hz
	Duration	8 s
Action	Sequence length	256 tokens
Box	Coordinates	(x_1, y_1, x_2, y_2)

Table 2. Training data configurations.

provisioned can be flexibly combined to form diverse MMs. Regarding the training input data, as shown in Table 2, we apply the data preparation methods discussed in Sec. 3.5 to enforce a uniform (yet modal-specific) sample length (size) for each module; all are typical values suggested by their official documentations. The training batch size is by default set to 32 and degrades to 16 for single-node experiments.

Baselines and metrics. We compare *Mosaic* with the three baselines previously elaborated in Sec. 2.2: *Megatron-LM* [54], *DistMM* [21], and *Spindle* [67]. Our primary metric to evaluate the training efficiency is the *per-iteration training makespan*. Additionally, we report hardware efficiency via *Compute-Warps-in-Flight* [44]¹.

5.2 End-to-End Performance

Fig. 9 depicts the average per-iteration time of each MM under different deployment methods. It confirms that *Mosaic* consistently achieves the best training efficiency, with $1.07\times$ – $1.31\times$ speedup over *Spindle* (the second best), $1.10\times$ – $1.42\times$ over *DistMM*, and $1.17\times$ – $1.48\times$ over *Megatron-LM*. Such superiority aligns with our previous analysis in Sec. 2.2. Moreover, we also notice that the performance benefit of *Mosaic* is relatively larger for more complex MMs: the improvement of *Mosaic* over *Spindle* is $1.07\times$ for CLIP, yet it is $1.31\times$ for OFASys (which has 9 encoder modules). This is because for MMs with substantially heterogeneous modules, enforcing full-GPU allocation, as done in existing works, would render some GPUs highly underutilized.

To confirm, we further resort to the average per-GPU utilization information shown in Fig. 10. It suggests that

¹We avoid the misleading coarse-grained GPU Utilization as it only reflects whether any kernel is active and may remain high even when SM resources are under-saturated. In contrast, *Compute-Warps-in-Flight* directly reflects the amount of compute-active warps on SMs, making it a better indicator.

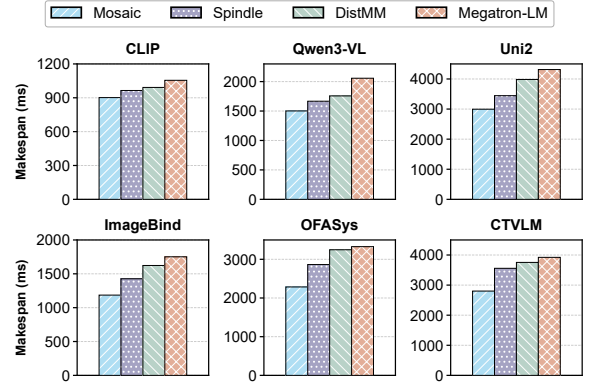


Figure 9. Per-iteration time when training different MMs.

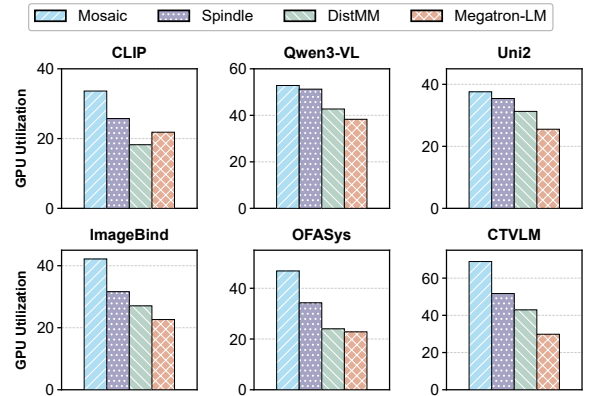


Figure 10. GPU utilization when training different MMs.

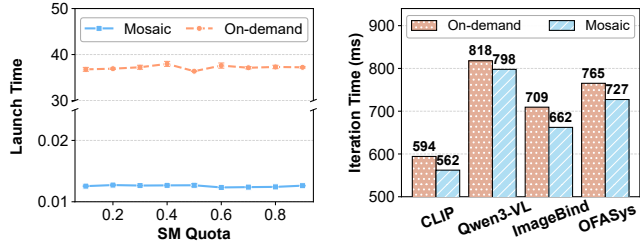
Mosaic does achieve the highest GPU utilization for all the models: on average, the GPU utilization under *Mosaic* is 47.0%, yet under *Spindle*, *DistMM*, and *Megatron-LM*, they are respectively 38.3%, 31.0%, and 26.8%. In particular, for the highly-heterogeneous OFASys model, the most underutilized GPU under *Spindle*, which hosts the *IMU* module, has a utilization of 24.7%, yet under *Mosaic* that utilization is increased to 56.3%. This demonstrates that, by enabling spatial multiplexing, *Mosaic* effectively enhances the overall GPU utilization, thereby improving the MM training efficiency.

5.3 Microscopic Performance Deep Dive

In this part, we respectively study the effectiveness of a series of techniques adopted in *Mosaic*.

5.3.1 Superiority of *Mosaic* Multiplexing Engine.

Recall that in Sec. 3.2, to mitigate the runtime provisioning overhead of diverse GC-streams, we propose to pre-create a pool of GC-streams with the desired quotas. To check its necessity, we measure the average time overhead to create GC-stream of different SM quotas (from 0.1 to 0.9; each point is repeated 30 times, and the error-bars show the upper/lower



(a) GC-stream preparation latency under different schemes. (b) End-to-end iteration time under different schemes.

Figure 11. GC-stream pre-creation remarkably reduces provision latency and benefits end-to-end iteration time.

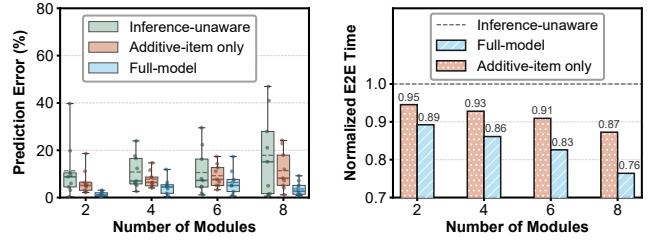
bounds). As shown in Fig. 11a, on-demand GC-stream creation takes a time overhead of around 37 ms; in contrast, by creating the GC-streams a priori, the amortized GC-stream launching overhead shrinks to around 0.013 ms, achieving a remarkable overhead reduction.

We further evaluate how this GC-stream launching speedup translates to the end-to-end performance benefit. Fig. 11b compares the average per-iteration time of four typical MMs (CLIP, Qwen3-VL, ImageBind, and OFASys) with and without GC-stream pre-creation. Across these workloads, *Mosaic* reduces end-to-end iteration time by 2.4%–6.6%, with an average reduction of about 4.6%. This confirms that such a technique is indispensable to *Mosaic* performance superiority.

5.3.2 Superiority of *Mosaic* Performance Model.

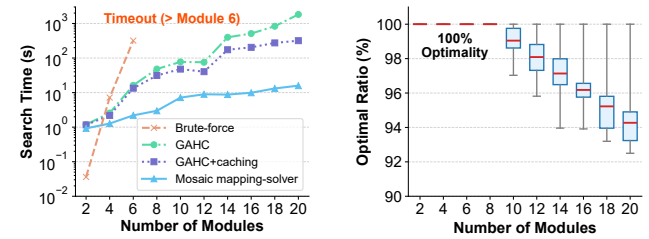
Recall that in Sec. 3.3, we have built an interference-aware performance model which includes both the *additive* and *multiplicative* items. To confirm the superiority of that performance model, we resort to the ablation study depicted in Fig. 12a, in which we evaluate the modeling accuracy for the OFASys model by setting up varying module numbers. Specifically, we evaluate three modeling schemes: (1) *inference-unaware*, which directly uses the per-module scaling surfaces, (2) *additive-item only*, which only includes the additive item when fitting the performance model, and (3) *full model*, which uses the full model depicted by Eq. 8. The ground-truth latency is obtained by actually executing each tested colocation plan. As shown in Fig. 12a, the *full-model* method consistently attains the highest modeling accuracy. For example, with 8 modules in the OFASys model, it attains an average prediction error of merely 3.65%, much smaller than the other methods (11.39% and 17.85%, respectively). This confirms the superiority of our performance model in Eq. 8.

In Fig. 12b, we further show the resultant per-iteration time of the OFASys model under different performance modeling methods; all results are normalized by the value under



(a) Prediction error across different modeling strategies. (b) Normalized E2E time under different modeling strategies.

Figure 12. *Mosaic*'s interference-aware performance model outperforms the other baseline methods in both prediction error and end-to-end performance.



(a) Search time ablation study. (b) Quality of *Mosaic*'s solution compared to genuine optimal from exhaustive enumeration.

Figure 13. *Mosaic*'s search algorithm finds near-optimal solution with high time efficiency.

the *inference-unaware* performance model. Fig. 12b reveals that the performance model in Eq. 8 achieves a training speedup of 11%–24%. Moreover, that speedup level increases when the OFASys model comprises more modules, because with more modules, the cross-module performance interference is more salient. In summary, our interference-aware performance model is crucial to the superiority of *Mosaic*.

5.3.3 Superiority of *Mosaic* Mapping Solver.

Recall that in Sec. 3.4, to solve the *module-stage* mapping and *module-GPU* mapping problem, we apply the GAHC heuristic and also incorporate *early-pruning* and *result-caching* for better efficiency. To confirm the effectiveness of those methods, we compare the efficiency and quality performance of *Mosaic* mapping-solver (Alg. 1) against multiple baselines: (1) *brute-force*, which finds the best mapping scheme by exhaustive grid search, (2) *GAHC*, which uses the standard GAHC algorithm without pruning or caching, (3) *GAHC+caching*, which further incorporates result caching into GAHC, and (4) *Mosaic mapping-solver*, which incorporates both early-pruning and result-caching with GAHC.

Fig. 13a shows the search time of the optimal deployment plan for the OFASys model (under varying module number). According to Fig. 13a, as the module number increases, the *brute-force* method quickly becomes intractable (surpassing the time budget of 1800s). By contrast, all the other methods can find the optimal solution within the time budget for up to 20 modules. In particular, the *Mosaic mapping-solver*, which combines GAHC with both early-pruning and result-caching, attains the best efficiency; this demonstrates the necessity of the two techniques.

Meanwhile, regarding the solution quality, as suggested in Fig. 13b (the optimal plan is obtained by exhaustive search), the deployment plan found by our *Mosaic* mapping-solver achieves 100% optimality (in per-iteration time) for up to 4 modules, and remains near-optimal as the search space grows. The median optimality ratio is around 94.27% with 10 modules. Therefore, *Mosaic* mapping-solver performs well in both solution efficiency and quality.

5.4 Sensitivity Analysis

5.4.1 Sensitivity to GPU Cluster Scale.

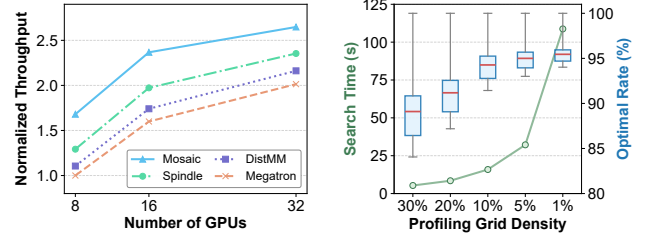
We first examine whether *Mosaic* remains effective as the available resource pool scales. This experiment fixes a four-module *OFASys* workload, varies the GPU pool size from 8 to 32 GPUs and compares their throughput (defined as $\frac{1}{\text{iteration time}}$). As shown in Fig. 14a, *Mosaic* consistently achieves the highest throughput across all evaluated GPU pool sizes. Compared with *Megatron-LM* under the same GPU pool size, *Mosaic* improves throughput by 1.68 \times , 1.48 \times , and 1.31 \times on 8, 16, and 32 GPUs, respectively. Against the strongest baseline, *Spindle*, the corresponding speedups are 1.30 \times , 1.20 \times , and 1.12 \times ; against *DistMM*, they are 1.52 \times , 1.36 \times , and 1.22 \times .

This trend indicates that spatial multiplexing is particularly valuable when the GPU pool is tight. With fewer GPUs, integer and exclusive-GPU allocation policies have less room to absorb module-level imbalance, so lightweight modules are more likely to leave sub-GPU compute capacity unused. *Mosaic* instead allows complementary modules to share GPUs with fractional SM quotas, improving aggregate throughput under the same resource budget. As the GPU pool grows, the relative pressure on each allocation decision decreases, and the speedup gradually narrows, but *Mosaic* still preserves the best throughput at every scale.

5.4.2 Sensitivity to SM-quota Search Granularity.

We next study the effect of the *SM-quota search granularity* introduced in Sec. 3.4, to understand how *Mosaic* balances search time and solution quality.

Fig. 14b reports the resulting search time and median optimality ratio compared to the optimal plan found by exhaustive enumeration. Coarse granularities substantially reduce search overhead but compromise the solution quality: at 30% and 20%, the search finishes in 5.32 s and 8.46 s, while



(a) Throughput under different GPU cluster scales. (b) Search-time/quality trade-off under different SM-quota search granularities.

Figure 14. Sensitivity of *Mosaic* to cluster scale and SM-quota search granularity on the OFASys model.

the median optimality ratio is only 89.10% and 91.18%. Reducing the granularity to 10% (the default value for main experiments) improves the median optimality ratio to 94.27% with a moderate 15.87 s search time, forming a practical knee point in the trade-off. Further refining the search granularity brings limited additional benefit. Compared with 10%, the 5% and 1% settings make the search 2.03 \times and 6.85 \times slower, respectively, but improve median optimality by only 0.73 and 1.18 percentage points. These results suggest that a 10% SM-quota search granularity captures most of the benefit of fine-grained spatial allocation while avoiding the rapidly increasing overhead of near-continuous search.

6 Related Works

In this section, we present other related works additional to those we have mentioned in Sec. 2.2, in aspects respectively in distributed model deployment, spatial GPU multiplexing and efficient training of large-scale MMs.

Distributed model deployment. With the increasing use of neural network models, deploying large neural network models on distributed GPUs has been a hot research topic in the literature. Apart from the traditional DP [30], TP [54] and PP [22, 39] parallelization schemes which are elaborated in Sec. 2.1, recently some new parallelization schemes also emerge, including *Sequence Parallel* (SP) [29], *Context Parallel* (CP) [33] and *Expert Parallel* (EP) [51]. Meanwhile, given the increasing model deployment complexity, a series of auto-parallelization works, like *Alpa* [82] and *Metis* [65] have also been proposed. However, these works commonly focus on Large Language Models, which are highly symmetric and executed in a purely sequential manner; their parallelization methods are over-simplified for MMs that have multiple heterogeneous module branches.

Spatial GPU Multiplexing. Spatial GPU multiplexing has been widely studied to improve GPU utilization, overwhelmingly for inference acceleration. For example, *Salus* [75] provides fine-grained GPU sharing primitives for DL applications, *REEF* [18] enables microsecond-scale preemption for concurrent DNN inferences, *Orion* [58] further improves GPU sharing performance for ML applications through interference-aware scheduling, and *MuxServe* [11] exploits spatial-temporal multiplexing for LLM serving. To the best of our knowledge, we are the first that exploit spatial GPU multiplexing to speed up the training efficiency of emerging MMs.

Efficient training of large-scale, cloud-grade MMs. Deploying large-scale, cloud-grade MMs in hundreds or thousands of GPUs has been the research focus of a series of recent works. For example, *Cornstarch* [24], *Optimus* [12], *GraphPipe* [25], *PipeWeaver* [72], and *MegaScale-Omni* [71] all seek to advance the parallelization schemes for such large-scale MMs, for which PP optimization (against module and data heterogeneity) is the key focus. By contrast, in this paper, we focus on *edge-grade* MMs, which would be even more significant than cloud-grade MMs in terms of the entity number and scenario diversity [37]. Meanwhile, as elaborated in Sec. 3.5, our temporal-spatial multiplexing method can be jointly applied with more advanced parallelization schemes (exemplified by PP) when training large MMs.

7 Conclusion

This paper introduced *Mosaic*, a system for efficient training of MMs comprising heterogeneous modules. Motivated by the growing module heterogeneity of modern multimodal models, *Mosaic* maps dependent modules into sequential stages while allowing parallel modules within each stage to share GPUs with fine-grained SM allocations. *Mosaic* realizes this approach with three coordinated components: a flexible GreenContext-based multiplexing engine, a performance model that captures scaling behavior and colocation interference, and a mapping solver that efficiently finds high-quality temporal and spatial deployment plans. Our evaluation on representative MMs and a 32-H100 cluster shows that *Mosaic* consistently improves GPU utilization, achieving up to 1.31 \times training-efficiency improvement over existing methods. Overall, *Mosaic* shows that carefully planned temporal-spatial multiplexing can effectively reduce cross-module bubbles and unlock underutilized GPU resources in MM training.

References

- [1] ACHIAM, J., ADLER, S., AGARWAL, S., AHMAD, L., AKKAYA, I., ALEMAN, F. L., ALMEIDA, D., ALTENSCHMIDT, J., ALTMAN, S., ANADKAT, S., ET AL. Gpt-4 technical report. *arXiv preprint arXiv:2303.08774* (2023).
- [2] BAI, J., ET AL. Ofasys: A multi-modal multi-task learning system for building generalist models. *arXiv*, 2022. *arXiv:2212.04408*.
- [3] BAI, S., CAI, Y., CHEN, R., ET AL. Qwen3-v1 technical report. *arXiv*, 2025. *arXiv:2511.21631*.
- [4] BÖTHER, M., ROBROEK, T., GSTEIGER, V., HOLZINGER, R., MA, X., TÖZÜN, P., AND KLIMOVIC, A. Modyn: Data-centric machine learning pipeline orchestration. *Proc. ACM Manag. Data* 3, 1 (Feb. 2025).
- [5] CARON, M., TOUVRON, H., MISRA, I., JÉGOU, H., MAIRAL, J., BOJANOWSKI, P., AND JOULIN, A. Emerging properties in self-supervised vision transformers. In *Proceedings of the IEEE/CVF International Conference on Computer Vision* (2021), pp. 9650–9660.
- [6] CHEN, W., LI, Z., AND XIN, S. Omnivlm: A token-compressed, sub-billion-parameter vision-language model for efficient on-device inference, 2024.
- [7] CHEN, Z., WANG, W., CAO, Y., ET AL. Expanding performance boundaries of open-source multimodal models with model, data, and test-time scaling. *arXiv*, 2024. *arXiv:2412.05271*.
- [8] DOSOVITSKIY, A., BEYER, L., KOLESNIKOV, A., WEISSENBORN, D., ZHAI, X., UNTERTHINER, T., DEGHANI, M., MINDERER, M., HEIGOLD, G., GELLY, S., USZKOREIT, J., AND HOULSBY, N. An image is worth 16x16 words: Transformers for image recognition at scale. In *International Conference on Learning Representations* (2021).
- [9] DRAPER, N. R., AND SMITH, H. *Applied Regression Analysis*, 3 ed. John Wiley & Sons, 1998.
- [10] DRIESS, D., XIA, F., SAJJADI, M. S. M., LYNCH, C., CHOWDHURY, A., ICHTER, B., WAHID, A., TOMPSON, J., VUONG, Q., YU, T., HUANG, W., CHEBOTAR, Y., SERMANET, P., DUCKWORTH, L., LEVINE, S., VANHOUCQUE, V., HAUSMAN, K., TOUSSAINT, M., GREFF, K., ZENG, A., MORDATCH, I., AND FLORENCE, P. PaLM-e: An embodied multimodal language model. In *Proceedings of the 40th International Conference on Machine Learning* (23–29 Jul 2023), A. Krause, E. Brunskill, K. Cho, B. Engelhardt, S. Sabato, and J. Scarlett, Eds., vol. 202 of *Proceedings of Machine Learning Research*, PMLR, pp. 8469–8488.
- [11] DUAN, J., LU, R., DUANMU, H., LI, X., ZHANG, X., LIN, D., STOICA, I., AND ZHANG, H. MuxServe: Flexible spatial-temporal multiplexing for multiple LLM serving. In *Proceedings of the 41st International Conference on Machine Learning* (2024), vol. 235 of *Proceedings of Machine Learning Research*, PMLR, pp. 11905–11917.
- [12] FENG, W., CHEN, Y., WANG, S., PENG, Y., LIN, H., AND YU, M. Optimus: Accelerating {Large-Scale} {Multi-Modal} {LLM} training by bubble exploitation. In *2025 USENIX Annual Technical Conference (USENIX ATC 25)* (2025), pp. 161–177.
- [13] GARG, S., FARAJTABAR, M., POURANSARI, H., VEMULAPALLI, R., MEHTA, S., TUZEL, O., SHANKAR, V., AND FAGHRI, F. Tic-clip: Continual training of clip models. In *International Conference on Learning Representations* (2024), B. Kim, Y. Yue, S. Chaudhuri, K. Fragkiadaki, M. Khan, and Y. Sun, Eds., vol. 2024, pp. 16649–16684.
- [14] GE, C., WANG, X., ZHANG, Z., CHEN, H., FAN, J., HUANG, L., XUE, H., AND ZHU, W. Dynamic mixture of curriculum LoRA experts for continual multimodal instruction tuning. In *Proceedings of the 42nd International Conference on Machine Learning* (13–19 Jul 2025), A. Singh, M. Fazel, D. Hsu, S. Lacoste-Julien, F. Berkenkamp, T. Maharaj, K. Wagstaff, and J. Zhu, Eds., vol. 267 of *Proceedings of Machine Learning Research*, PMLR, pp. 19011–19033.
- [15] GEMINI TEAM, GOOGLE. Gemini 2.5: Pushing the frontier with advanced reasoning, multimodality, long context, and next generation agentic capabilities. Technical report, 2025.
- [16] GIRDHAR, R., EL-NOUBY, A., LIU, Z., SINGH, M., ALWALA, K. V., JOULIN, A., AND MISRA, I. Imagebind: One embedding space to bind them all. In *Proceedings of the IEEE/CVF Conference on Computer Vision and Pattern Recognition* (2023).
- [17] GOOGLE DEEPMIND. Gemini 3.1 Pro model card. Model card, 2026.
- [18] HAN, M., ZHANG, H., CHEN, R., AND CHEN, H. Microsecond-scale preemption for concurrent gpu-accelerated dnn inferences. In *16th USENIX Symposium on Operating Systems Design and Implementation (OSDI 22)* (2022), USENIX Association, pp. 539–558.
- [19] HE, Y., AND ET AL. LLMStation: Resource multiplexing in tuning and serving large language models. In *Proceedings of the 2025 USENIX*

- Annual Technical Conference* (2025), USENIX Association.
- [20] HEGDE, D., YASARLA, R., CAI, H., HAN, S., BHATTACHARYYA, A., MAHAJAN, S., LIU, L., GARREBALLI, R., PATEL, V. M., AND PORIKLI, F. Distilling multi-modal large language models for autonomous driving. In *Proceedings of the IEEE/CVF Conference on Computer Vision and Pattern Recognition (CVPR)* (June 2025), pp. 27575–27585.
- [21] HUANG, J., ZHANG, Z., ZHENG, S., QIN, F., AND WANG, Y. {DISTMM}: Accelerating distributed multimodal model training. In *21st USENIX Symposium on Networked Systems Design and Implementation (NSDI 24)* (2024), pp. 1157–1171.
- [22] HUANG, Y., CHENG, Y., BAPNA, A., FIRAT, O., CHEN, M., CHEN, D., LEE, H., NGIAM, J., LE, Q. V., WU, Y., AND CHEN, Z. Gpipe: Efficient training of giant neural networks using pipeline parallelism. In *Advances in Neural Information Processing Systems (NeurIPS)* (2019). arXiv:1811.06965.
- [23] HUANG, Z., HE, Y., YU, J., ZHANG, F., SI, C., JIANG, Y., ZHANG, Y., WU, T., JIN, Q., CHANPAISIT, N., WANG, Y., CHEN, X., WANG, L., LIN, D., QIAO, Y., AND LIU, Z. VBench: Comprehensive benchmark suite for video generative models. In *Proceedings of the IEEE/CVF Conference on Computer Vision and Pattern Recognition* (2024).
- [24] JANG, I., LU, R., BANSAL, N., CHEN, A., AND CHOWDHURY, M. Efficient distributed MLLM training with Cornstarch, 2025.
- [25] JEON, B., WU, M., CAO, S., KIM, S., PARK, S., AGGARWAL, N., UNGER, C., ARFEEN, D., LIAO, P., MIAO, X., ALIZADEH, M., GANGER, G. R., CHEN, T., AND JIA, Z. Graphpipe: Improving performance and scalability of dnn training with graph pipeline parallelism. In *Proceedings of the 30th ACM International Conference on Architectural Support for Programming Languages and Operating Systems (ASPLOS)* (2025).
- [26] KIM, M. J., PERTSCH, K., KARAMCHETI, S., XIAO, T., BALAKRISHNA, A., NAIR, S., RAFAILOV, R., FOSTER, E. P., SANKETI, P. R., VUONG, Q., KOLLAR, T., BURCHFIELD, B., TEDRAKE, R., SADIGH, D., LEVINE, S., LIANG, P., AND FINN, C. OpenVLA: An open-source vision-language-action model. In *Proceedings of The 8th Conference on Robot Learning* (2025), vol. 270 of *Proceedings of Machine Learning Research*, PMLR, pp. 2679–2713.
- [27] KRELL, M. M., KOSEC, M., PEREZ, S. P., AND FITZGIBBON, A. Efficient sequence packing without cross-contamination: Accelerating large language models without impacting performance. *arXiv preprint arXiv:2107.02027* (2022).
- [28] LI, B., LI, Y., LI, Z., LIU, C., LIU, W., NIU, G., TAN, Z., XU, H., YAO, Z., YUAN, T., ZHOU, D., ZHUANG, Y., YAN, S., DAI, G., AND WANG, Y. Megrez-omni technical report, 2025.
- [29] LI, S., XUE, F., BARANWAL, C., LI, Y., AND YOU, Y. Sequence parallelism: Long sequence training from system perspective. *arXiv preprint arXiv:2105.13120* (2021).
- [30] LI, S., ZHAO, Y., VARMA, R., SALPEKAR, O., NOORDHUIS, P., LI, T., PASZKE, A., SMITH, J., VAUGHAN, B., DAMANIA, P., ET AL. Pytorch distributed: Experiences on accelerating data parallel training. *arXiv preprint arXiv:2006.15704* (2020).
- [31] LIU, C., QIAN, Y., TANG, D., ZHU, H., PANG, J., AND CAI, Q. From insight to action: Embodied multi-agent system integrating vision language model for digital twin-assisted human-robot collaborative assembly. *Journal of Manufacturing Systems* 85 (2026), 531–556.
- [32] LIU, H., LI, C., WU, Q., AND LEE, Y. J. Visual instruction tuning. *Advances in neural information processing systems* 36 (2023), 34892–34916.
- [33] LIU, H., ZAHARIA, M., AND ABBEEL, P. Ring attention with blockwise transformers for near-infinite context. In *The Twelfth International Conference on Learning Representations* (2024).
- [34] LIU, Z., DONG, Y., WANG, J., LIU, Z., HU, W., LU, J., AND RAO, Y. Ola: Pushing the frontiers of omni-modal language model. *arXiv preprint arXiv:2502.04328* (2025).
- [35] LU, J., CLARK, C., LEE, S., ZHANG, Z., KHOSLA, S., MARTEN, R., HOIEM, D., AND KEMBHAVI, A. Unified-io 2: Scaling autoregressive multimodal models with vision, language, audio, and action. In *Proceedings of the IEEE/CVF Conference on Computer Vision and Pattern Recognition* (2024).
- [36] LU, S., GUO, L., WANG, W., ZHAO, Z., YUE, T., LIU, J., AND LIU, S. Collaborative training of tiny-large vision language models. In *Proceedings of the 32nd ACM International Conference on Multimedia* (2024), pp. 4928–4937.
- [37] MARKETANDMARKETS. Edge ai software market worth 8.89 billion by 2031. Web Page, 2026.
- [38] MOONSHOT AI. Kimi K2.5: Visual agentic intelligence. Technical blog, 2026.
- [39] NARAYANAN, D., HARLAP, A., PHANISHAYEE, A., SESHADRI, V., DEVANUR, N. R., GANGER, G. R., GIBBONS, P. B., AND ZAHARIA, M. Pipedream: Generalized pipeline parallelism for dnn training. In *Proceedings of the 27th ACM Symposium on Operating Systems Principles (SOSP)* (2019).
- [40] NVIDIA. Multi-instance gpu user guide. NVIDIA Documentation, 2025. Accessed 2026-01-20.
- [41] NVIDIA. Cuda c++ programming guide. <https://docs.nvidia.com/cuda/cuda-c-programming-guide/>, 2026.
- [42] NVIDIA CORPORATION. Cuda c++ programming guide: Green contexts. <https://docs.nvidia.com/cuda/cuda-programming-guide/04-special-topics/green-contexts.html>, 2025. Accessed: 2026-02-04.
- [43] NVIDIA CORPORATION. Cuda multi-process service (mps) overview. https://docs.nvidia.com/deploy/pdf/CUDA_Multi_Process_Service_Overview.pdf, 2025. Accessed: 2026-02-04.
- [44] NVIDIA CORPORATION. *NVIDIA Nsight Systems User Guide: GPU Metrics*. NVIDIA Corporation, 2026. Version 2026.2.
- [45] OPENAI. Introducing GPT-5.4. OpenAI product release, 2026.
- [46] PASZKE, A., GROSS, S., MASSA, F., LERER, A., BRADBURY, J., CHANAN, G., KILLEEN, T., LIN, Z., GIMELSHEIN, N., ANTIGA, L., ET AL. Pytorch: An imperative style, high-performance deep learning library. *Advances in neural information processing systems* 32 (2019).
- [47] PERRON, L., AND FURNON, V. Or-tools.
- [48] PORTES, J., TROTT, A., HAVENS, S., KING, D., VENIGALLA, A., NADEEM, M., SARDANA, N., KHUDIA, D., AND FRANKLE, J. Mosaicbert: A bidirectional encoder optimized for fast pretraining. In *Advances in Neural Information Processing Systems* (2023), vol. 36.
- [49] QWEN TEAM. Qwen3.5-397B-A17B model card. Hugging Face model card, 2026.
- [50] RADFORD, A., KIM, J. W., HALLACY, C., RAMESH, A., GOH, G., AGARWAL, S., SASTRY, G., ASKELL, A., MISHKIN, P., CLARK, J., KRUEGER, G., AND SUTSKEVER, I. Learning transferable visual models from natural language supervision. In *Proceedings of the 38th International Conference on Machine Learning* (2021), M. Meila and T. Zhang, Eds., vol. 139 of *Proceedings of Machine Learning Research*, PMLR, pp. 8748–8763.
- [51] RAJBHANDARI, S., LI, C., YAO, Z., ZHANG, M., AMINABADI, R. Y., AWAN, A. A., RASLEY, J., AND HE, Y. DeepSpeed-MoE: Advancing mixture-of-experts inference and training to power next-generation AI scale. In *Proceedings of the 39th International Conference on Machine Learning* (2022), vol. 162 of *Proceedings of Machine Learning Research*, PMLR, pp. 18332–18346.
- [52] RAO, Y., ZHAO, W., LIU, B., LU, J., ZHOU, J., AND HSIEH, C.-J. Dynamicvit: Efficient vision transformers with dynamic token sparsification. In *Advances in Neural Information Processing Systems* (2021), vol. 34.
- [53] SHAO, Z., YU, Z., YU, J., OUYANG, X., ZHENG, L., GAI, Z., WANG, M., KUANG, Z., AND DING, J. Imp: Highly capable large multimodal models for mobile devices. *IEEE Transactions on Multimedia* 27 (2025), 2961–2974.
- [54] SHOEBY, M., PATWARY, M., PURI, R., LEGRÉSLEY, P., CASPER, J., AND CATANZARO, B. Megatron-lm: Training multi-billion parameter language models using model parallelism. *arXiv preprint arXiv:1909.08053* (2019).
- [55] SHUBHA, S. S., SHEN, H., AND IYER, A. USHER: Holistic interference avoidance for resource optimized ML inference. In *18th USENIX Symposium on Operating Systems Design and Implementation (OSDI 24)* (2024), USENIX Association, pp. 947–964.

- [56] SIMA, C., RENZ, K., CHITTA, K., CHEN, L., ZHANG, H., XIE, C., BEISSWENGER, J., LUO, P., GEIGER, A., AND LI, H. DriveLM: Driving with graph visual question answering. In *Computer Vision – ECCV 2024* (2024), Springer, pp. 256–274.
- [57] SIRU, C., YUANCHAO, S., CONG, W., AND JIMING, C. A survey on edge multimodal large models: compression, inference acceleration, and applications. *National Science Open*.
- [58] STRATI, F., MA, X., AND KLIMOVIC, A. Orion: Interference-aware, fine-grained gpu sharing for ml applications. In *Proceedings of the Nineteenth European Conference on Computer Systems* (2024), EuroSys '24, Association for Computing Machinery, pp. 1075–1092.
- [59] TEAM, Q. Qwen3. 5-omni technical report. *arXiv preprint arXiv:2604.15804* (2026).
- [60] TEED, Z., AND DENG, J. RAFT: Recurrent all-pairs field transforms for optical flow. In *Proceedings of the European Conference on Computer Vision* (2020), pp. 402–419.
- [61] THE BUSINESS RESEARCH COMPANY. On-device multimodal ai market report 2026. Market report, 2026.
- [62] TIAN, X., GU, J., LI, B., LIU, Y., WANG, Y., ZHAO, Z., ZHAN, K., JIA, P., LANG, X., AND ZHAO, H. Drivevlm: The convergence of autonomous driving and large vision-language models. In *Proceedings of The 8th Conference on Robot Learning* (06–09 Nov 2025), P. Agrawal, O. Kroemer, and W. Burgard, Eds., vol. 270 of *Proceedings of Machine Learning Research*, PMLR, pp. 4698–4726.
- [63] TSCHANNEN, M., ET AL. Siglip 2: Multilingual vision-language encoders with improved semantic understanding. *arXiv*, 2025. arXiv:2502.14786.
- [64] UDANDARAO, V., ROTH, K., DZIADZIO, S., PRABHU, A., CHERTI, M., VINYALS, O., HÉNAFF, O., ALBANIE, S., AKATA, Z., AND BETHGE, M. A practitioner’s guide to real-world continual multimodal pretraining. In *Advances in Neural Information Processing Systems* (2024), A. Globerson, L. Mackey, D. Belgrave, A. Fan, U. Paquet, J. Tomczak, and C. Zhang, Eds., vol. 37, Curran Associates, Inc., pp. 133801–133845.
- [65] UM, T., OH, B., KANG, M., LEE, W.-Y., KIM, G., KIM, D., KIM, Y., MUZZAMMIL, M., AND JEON, M. Metis: Fast automatic distributed training on heterogeneous GPUs. In *2024 USENIX Annual Technical Conference (USENIX ATC 24)* (Santa Clara, CA, July 2024), USENIX Association, pp. 563–578.
- [66] WANG, Y., WANG, Y., CHEN, C., XUE, C., WENG, Q., CHEN, Y., LI, Z., ZHU, X., YANG, Y., CHEN, Q., ET AL. Suika: Efficient and high-quality re-scheduling of 3d-parallelized llm training jobs in shared clusters. In *Proceedings of the 21st European Conference on Computer Systems* (2026), pp. 2002–2021.
- [67] WANG, Y., ZHU, S., FU, F., MIAO, X., ZHANG, J., ZHU, J., HONG, F., LI, Y., AND CUI, B. Spindle: Efficient distributed training of multi-task large models via wavefront scheduling. *arXiv*, 2024. arXiv:2409.03365.
- [68] WEN, Z., GAO, Y., LI, W., HE, C., AND ZHANG, L. Token pruning in multimodal large language models: Are we solving the right problem?, 2025. Findings of ACL 2025.
- [69] WU, Y., LI, D., CHEN, Y., JIANG, R., ZOU, H. P., HUANG, W.-C., LI, Y., FANG, L., WANG, Z., AND YU, P. S. Multi-agent autonomous driving systems with large language models: A survey of recent advances, resources, and future directions. *Findings of the Association for Computational Linguistics: EMNLP 2025* (2025).
- [70] XU, Z., ZHANG, Y., XIE, E., ZHAO, Z., GUO, Y., WONG, K.-Y. K., LI, Z., AND ZHAO, H. Drivegpt4: Interpretable end-to-end autonomous driving via large language model. *IEEE Robotics and Automation Letters* 9, 10 (2024), 8186–8193.
- [71] XUE, C., CHEN, Y., JIANG, J., ZHENG, N., FENG, J., CHEN, J., ZHAO, S., YAN, S., LIN, Y., SHI, L., ET AL. Megascale-omni: A hyper-scale, workload-resilient system for multimodal llm training in production. In *Proceedings of the 21st European Conference on Computer Systems* (2026), pp. 675–692.
- [72] XUE, Z., HU, H., CHEN, X., JIANG, Y., SONG, Y., MI, Z., ZHU, Y., JIANG, D., XIA, Y., AND CHEN, H. Pipeweaver: Addressing data dynamicity in large multimodal model training with dynamic interleaved pipeline. *arXiv*, 2025. arXiv:2504.14145.
- [73] YAO, Y., YU, T., ZHANG, A., WANG, C., CUI, J., ZHU, H., CAI, T., CHEN, C., LI, H., ZHAO, W., HE, Z., CHEN, Q., ZHOU, R., ZOU, Z., ZHANG, H., HU, S., ZHENG, Z., ZHOU, J., CAI, J., HAN, X., ZENG, G., LI, D., LIU, Z., AND SUN, M. Efficient GPT-4V level multimodal large language model for deployment on edge devices. *Nature Communications* 16, 1 (jul 2025), 5509.
- [74] YAO, Y., YU, T., ZHANG, A., WANG, C., CUI, J., ZHU, H., CAI, T., CHEN, C., LI, H., ZHAO, W., HE, Z., CHEN, Q., ZHOU, R., ZOU, Z., ZHANG, H., HU, S., ZHENG, Z., ZHOU, J., CAI, J., HAN, X., ZENG, G., LI, D., LIU, Z., AND SUN, M. Efficient GPT-4V level multimodal large language model for deployment on edge devices. *Nature Communications* 16, 5509 (2025).
- [75] YU, P., AND CHOWDHURY, M. Salus: Fine-grained gpu sharing primitives for deep learning applications. In *Proceedings of Machine Learning and Systems* (2020).
- [76] YURTSEVER, E., LAMBERT, J., CARBALLO, A., AND TAKEDA, K. A survey of autonomous driving: Common practices and emerging technologies. *IEEE access* 8 (2020), 58443–58469.
- [77] Z.AI. GLM-4.6. Technical blog, 2025.
- [78] ZHANG, D., QI, S., WU, Y., XIAO, X., WANG, X., AND CHEN, L. Fast-slow efficient training for multimodal large language models via visual token pruning, 2026.
- [79] ZHANG, S., XU, A., CHEN, Q., ZHAO, H., CUI, W., WANG, Z., LI, Y., XIAO, L., AND GUO, M. Efficient Performance-Aware GPU sharing with compatibility and isolation through kernel space interception. In *2025 USENIX Annual Technical Conference (USENIX ATC 25)* (2025), USENIX Association, pp. 1003–1019.
- [80] ZHAO, H., ZHU, F., GUO, H., WANG, M., WANG, R., MENG, G., AND ZHANG, Z. Mllm-cl: Continual learning for multimodal large language models, 2025.
- [81] ZHEN, H., QIU, X., CHEN, P., YANG, J., YAN, X., DU, Y., HONG, Y., AND GAN, C. 3D-VLA: A 3D vision-language-action generative world model. In *Proceedings of the 41st International Conference on Machine Learning* (2024), vol. 235 of *Proceedings of Machine Learning Research*, PMLR, pp. 61229–61245.
- [82] ZHENG, L., LI, Z., ZHANG, H., ZHUANG, Y., CHEN, Z., HUANG, Y., WANG, Y., XU, Y., ZHUO, D., XING, E. P., GONZALEZ, J. E., AND STOICA, I. Alpa: Automating inter- and Intra-Operator parallelism for distributed deep learning. In *16th USENIX Symposium on Operating Systems Design and Implementation (OSDI 22)* (Carlsbad, CA, July 2022), USENIX Association, pp. 559–578.
- [83] ZITKOVICH, B., YU, T., XU, S., XU, P., XIAO, T., XIA, F., WU, J., WOHLHART, P., WELKER, S., WAHID, A., VUONG, Q., VANHOUCHE, V., TRAN, H., SORICUT, R., SINGH, A., SINGH, J., SERMANET, P., SANKETI, P. R., SALAZAR, G., RYOO, M. S., REYMANN, K., RAO, K., PERTSCH, K., MORDATCH, I., MICHALEWSKI, H., LU, Y., LEVINE, S., LEE, L., LEE, T.-W. E., LEAL, I., KUANG, Y., KALASHNIKOV, D., JULIAN, R., JOSHI, N. J., IRPAN, A., ICHTER, B., HSU, J., HERZOG, A., HAUSMAN, K., GOPALAKRISHNAN, K., FU, C., FLORENCE, P., FINN, C., DUBEY, K. A., DRIESS, D., DING, T., CHOROMANSKI, K. M., CHEN, X., CHEBOTAR, Y., CARBAJAL, J., BROWN, N., BROHAN, A., ARENAS, M. G., AND HAN, K. Rt-2: Vision-language-action models transfer web knowledge to robotic control. In *Proceedings of The 7th Conference on Robot Learning* (06–09 Nov 2023), J. Tan, M. Toussaint, and K. Darvish, Eds., vol. 229 of *Proceedings of Machine Learning Research*, PMLR, pp. 2165–2183.